

Dynamics at an exceptional point in an interacting quantum dot system

William Samuelson



LUND
UNIVERSITY

A Bachelor's Thesis

Supervised by Martin Leijnse and Stephanie Matern

Division of Solid State Physics

Lund University

October 11, 2022

Dynamics at an exceptional point in an interacting quantum dot system

Abstract

A fundamental postulate of quantum mechanics is that the Hamiltonian of a closed system is Hermitian, guaranteeing real-valued energies and conserved probabilities throughout the evolution of the system. However, for quantum systems where there is dissipation and crosstalk with the environment, such as a system of quantum dots connected to an environment of metallic leads, the dynamics of the system is instead generated by a non-Hermitian Liouvillian superoperator. One feature of non-Hermitian operators, showing increasing theoretical and experimental interest recently, is the possibility of exceptional points. These are points in parameter space which cause two or more eigenvalues and their corresponding eigenvectors of the operator to simultaneously coalesce. Exceptional points can be of different orders, corresponding to the number of coalescing eigenvectors and eigenvalues. In this thesis, we study a system of two quantum dots coupled in parallel to metallic leads and demonstrate the existence of a second order exceptional point in the Liouvillian superoperator. Furthermore, the dynamics at this exceptional point is analyzed in detail using a combination of analytical and numerical methods, including simulations of the density operator and the current through the system. We show that the dynamics can be understood in terms of generalized modes and that the system exhibits unique algebraic decay at the exceptional point. Furthermore, critical damping at the exceptional point is indicated in the current, in accordance with a previous work on exceptional points in quantum thermal machines. We also briefly discuss possible applications of exceptional points in quantum dots, including control and sensing technologies.

Contents

1	Introduction	1
2	Background theory	4
2.1	Transport through quantum dots	4
2.2	The theory of open quantum systems	5
2.2.1	The von Neumann equation and the reduced density operator	6
2.2.2	The Lindblad Master equation	7
2.3	Exceptional points	8
2.3.1	Jordan normal form	8
2.3.2	General solution of linear ODEs	11
3	Results: EP-dynamics in a parallel dot system	13
3.1	Model	13
3.2	Spectrum	15
3.3	Dynamics	17
3.3.1	Varying initial conditions	18
3.3.2	Varying parameters	19
4	Conclusion and outlook	21
A	Derivation of Equation (2.20)	25

Chapter 1

Introduction

The theory of quantum mechanics developed in the last century has been proved to be extremely successful in describing nature at the small scale. Typical systems treated by quantum mechanics are nuclei, atoms, and other systems which can be assumed to be isolated from the environment. In such systems, the Hamiltonian is postulated to be Hermitian, guaranteeing that energies are real-valued and that the wave function is contained in the system throughout its evolution [1]. However, for many physical setups we cannot assume the system to be isolated and we must consider dissipation and the crosstalk between the system and its surroundings. One way to handle such open systems is to loosen the requirement of Hermiticity to include dissipation. The resulting field of non-Hermitian quantum physics has successfully been describing systems in nuclear, atomic and optical physics in recent decades [2]. One property of particular interest in non-Hermitian operators is the possibility of exceptional points (EPs). These correspond to points in parameter space where two or more eigenvalues and their corresponding eigenvectors of the operator simultaneously coalesce [3]. Exceptional points have been proposed to have several useful technological applications in e.g. optics and photonics [4, 5], and along with the optical microring experiments in 2017, EP sensors successfully increased the sensitivity of current measurements and nano-particle detection [6, 7]. These sensors exploit the fact that the eigenvalue splitting due to a small perturbation of the system is extra sensitive at an EP, compared with a degeneracy where only the eigenvalues coalesce.

A different framework which treats open systems is quantum master equations, where the dynamics of the system is generated by the Liouvillian superoperator [8]. Similarly to the Hamiltonian in non-Hermitian physics, the Liouvillian is non-Hermitian due to the coupling to the environment. However, in contrast to the non-Hermitian Hamiltonian where terms are added phenomenologically to take dissipation into account, the non-Hermiticity of the Liouvillian arises naturally when deriving a quantum master equation [9]. This non-Hermiticity brings the possibility of EPs also in the Liouvillian superoperator [10]. EPs in Liouvillian physics have been of particular theoretical interest recently, and are proposed to have important applications in control and sensing technologies. Two recent examples include Ref. [11], where critical decay towards the steady state in a quantum thermal machine was found at the EP; and Ref. [12] where an EP corresponded to optimal steering toward a target quantum state.

An application of particular interest for quantum master equations and Liouvil-

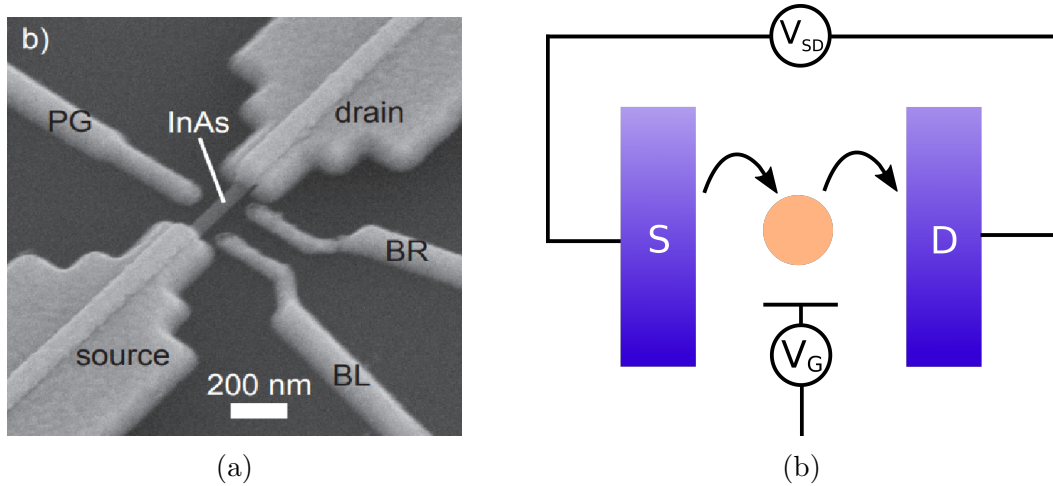


Figure 1.1: a) A physical implementation of a single QD system. The QD is realized within the InAs nanowire, with the source and drain, and the gates (BR, BL and PG) all clearly visible in this figure. The figure is taken from Ref. [16]. b) A schematic figure of a QD system where the QD is in the center, tunnel coupled to the source (S) and drain (D). The gate voltage V_G and the source-drain voltage V_{SD} , are tuned to define the QD.

lian physics is electron transport in systems of quantum dots connected to metallic leads [13]. A quantum dot (QD) is a fabricated semiconductor structure containing a small number of electrons and is typically in the order of 100 nanometres in size [14]. The size of the dot needs to be small in comparison to the thermal wavelength of the electrons, which is why experiments are generally realized at temperatures close to absolute zero [15]. One method of creating this tiny isolation of electrons is to confine them in nanowires. Nanowires are structures where two of the dimensions are on the nanometer scale and lengths of up to tens of micrometers [16]. This way, nanowires essentially act as a one-dimensional conductor. By then applying voltages via nanoscale electrodes, called gates, the number of electrons can be depleted in a small region, forming a QD, see Fig. 1.1a. If the voltages are tuned successfully, the QD can be tunnel coupled to the two surrounding conducting regions of the nanowire, known as the source and drain. The electrons can then tunnel from the source into the dot and then exiting it by tunneling into the drain, producing a current through the system [14]. This process is schematically presented in Fig. 1.1b.

There are many other ways of fabricating QDs which does not rely on gates or nanowires for confining the electrons. However, one general property of QDs is the tunability of their optical, electrical and chemical properties, which has made them useful in a large range of applications. Quantum dot technologies span areas from energy harvesting, display technologies, and sensors to medical and biological applications, with efficient lasers, biotags and solar harvesting devices being available on the market [17]. The transport setup given in Fig. 1.1 in particular, can be used as an extremely sensitive charge sensor, being able to detect transport of single electron charges [15]. The QD systems studied in the literature have also included systems containing multiple QDs in various arrangements. In Ref. [18] for example, a system with two QDs coupled in parallel was studied for its quantum interference effects in the transport dynamics, and was proposed to act as a sensitive electric switch.

In this thesis, a parallel QD system was studied for its non-equilibrium transport properties, with focus on the full quantum dynamics, including the transient current. In particular, the dynamics at a second order EP is analyzed in detail using a combination of numerical and analytical approaches. Summarizing the results from the thesis, a second order EP was found, after which we derive and numerically implement the transient dynamics of the parallel dot system at and away from the EP. The time evolution of the reduced density matrix in generalized modes is evidenced, including algebraic decay at the EP for certain initial conditions, as opposed to the exponential decay away from the EP. Furthermore, simulations of the current through the QDs indicated signatures of critical decay at the EP, similar to the study of quantum thermal machines in Ref. [11].

The thesis is divided in the following chapters. In Chapter 2 we present the underlying theory of the thesis, including electron transport in QD systems, tools used in the theory of open quantum systems, and the Jordan normal form, which is needed to construct the full dynamics at the EP. Chapter 3 consists of three parts. Firstly, a further description of the parallel QD system and the model used to describe it are given. Then, we calculate the Liouvillian and demonstrate the existence of a second order EP. Finally, the density matrix and the current through the system at the EP is simulated, and the transient behavior is analyzed in detail. In Chapter 4, we conclude and give an outlook on further work and open questions relevant to EPs in Liouvillian physics, and particularly in QD systems.

Chapter 2

Background theory

The theory chapter of the thesis is divided into three sections. Firstly, a brief overview of the theory behind transport through quantum dots is given. Then, the focus is turned to some of the tools used in open quantum systems, ultimately ending in a section about quantum master equations. The final section will further explain the notion of EPs, and introduce important tools used in EP physics. Throughout the entire thesis, we will set the reduced Planck constant, the Boltzmann constant and the elementary charge to unity, i.e., $\hbar = 1$, $k_b = 1$, and $|e| = 1$.

2.1 Transport through quantum dots

To understand the transport of electrons through a system of quantum dots, it is insightful to first study the single quantum dot system. The following explanation is inspired by Ref. [19].

Consider a single quantum dot with N electrons capacitively coupled to a gate, as well as to source and drain reservoirs through tunnel junctions as in Fig. 1.1b. The main transport properties of the system can then be understood in terms of the chemical potentials of the quantum dot and the source and drain reservoirs. These are often depicted in electro-chemical potential diagrams, see Fig. 2.1. There, $\mu(N)$ is the energy required to add the N th electron to the quantum dot, and μ_S and μ_D are the Fermi levels of the source and drain. The shaded areas represent the Fermi-Dirac distributions of the reservoirs.

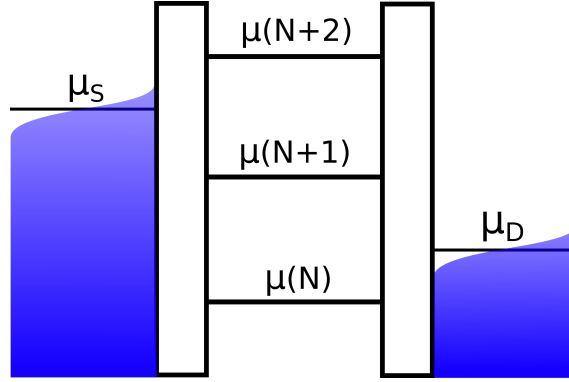


Figure 2.1: An electro-chemical potential diagram of the single quantum dot system. The source and drain are in a thermal distribution given by the shaded areas with Fermi levels μ_S and μ_D . The quantum dot is depicted as a ladder with energies $\mu(N)$, representing the energy required to add the N th electron to the dot. The figure is adapted from Ref. [19].

Using this picture, the electron transport through the quantum dot can be easily visualized. If the chemical potentials of the dot are located as in Fig. 2.1, $\mu(N+1)$ is below μ_S , and an electron will likely tunnel from the source onto the dot, increasing the number of electrons on the dot from N to $N+1$. After the tunneling event, there is an even lower chemical potential available for the electron, μ_D , and the electron will with a high probability leave the quantum dot and enter the drain. In this fashion, the system will cycle through having N and $N+1$ electrons on the dot, producing a current.

It turns out that $\mu(N)$ depends linearly on the gate voltage V_G . Consequently, the ladder of states in Fig. 2.1 can be lowered or raised by changing V_G . The source-drain voltage V_{SD} on the other hand, changes the difference between μ_S and μ_D . Through these two processes, it is possible to change the electro-chemical potential landscape and therefore control the current through the system. This captures the main behavior of the dynamics of the quantum dot system. However, by adapting the theory of open quantum systems, a much richer and more accurate theory can be developed.

2.2 The theory of open quantum systems

Open quantum systems are systems which are non-isolated and connected to some sort of environment. Often, it considers a total system consisting of the (sub)system of interest, and an environment. The total system is closed, and therefore it obeys the standard quantum mechanical equations of motion. The goal of the theory of open quantum systems is to infer the dynamics of the smaller system from the equations of the total system [20]. There are several approaches to open quantum systems, each with their own domain of applicability. In this thesis we will use a master equation approach, which handles electron-electron interactions in the system of interest well, but has the disadvantage of requiring approximations regarding the strength of the coupling to the environment. Another approach is by using Green's functions, which is relevant in the opposite domain, i.e., when there is strong coupling to the environment but negligible electron-electron interactions [21].

2.2.1 The von Neumann equation and the reduced density operator

An essential tool used in the theory of open quantum systems is the density operator $\hat{\rho}$. A common approach for such systems is to assume that the system is known to be in a state $|\psi_k\rangle$ with a probability p_k , or in another state $|\psi_l\rangle$ with a different probability p_l , and so on. Generally, the system is then said to be in an ensemble $\{|\psi_k\rangle, p_k\}_k$. The density operator describes this information in a compact way:

$$\hat{\rho} = \sum_k p_k |\psi_k\rangle \langle \psi_k|. \quad (2.1)$$

It can easily be shown that the density operator is Hermitian and has unity trace, since the probabilities must add up to one. Furthermore, by fixing a basis $\{|\phi_i\rangle\}$, the density operator can be represented by its matrix elements

$$\rho_{ij} = \langle \phi_i | \hat{\rho} | \phi_j \rangle = \sum_k p_k \langle \phi_i | \psi_k \rangle \langle \psi_k | \phi_j \rangle. \quad (2.2)$$

The diagonal elements ρ_{ii} represents classical probabilities of being in a state $|\phi_i\rangle$ and the off-diagonal elements ρ_{ij} are the so called coherences between state $|\phi_i\rangle$ and $|\phi_j\rangle$. Note that the matrix elements are basis dependent, and that there always is a basis in which the density operator is diagonal [8].

The average measured value of an observable \hat{O} of an ensemble represented by $\hat{\rho}$ is given by

$$\langle \hat{O} \rangle = \text{Tr}(\hat{\rho} \hat{O}). \quad (2.3)$$

From the density operator one can therefore extract all significant information from the ensemble, and it can be described as the "state" of the system. It is also possible to calculate how the density operator evolves over time. Under a Hamiltonian \hat{H} , the time evolution is given by the von Neumann equation

$$\frac{d\hat{\rho}}{dt} = i[\hat{\rho}, \hat{H}] \equiv \mathcal{L}\hat{\rho}, \quad (2.4)$$

where \mathcal{L} is the Liouvillian superoperator, or just the Liouvillian [8].

The Liouvillian \mathcal{L} in Eq. (2.4) is an operator acting on an operator, hence being called a superoperator. It is however possible to represent the Liouvillian as a matrix L , which acts on a vector representation of the density matrices, usually written as $|\rho\rangle\rangle$. The Hilbert space spanned by these vectors is called the Fock-Liouville space, equipped with a scalar product $\langle\langle \rho_1 | \rho_2 \rangle\rangle$ [20].

Returning to the mentioned goal of the theory of open quantum systems, a natural question is the following: How do we extract the density operator of a subsystem $\hat{\rho}_S$, from the total density operator $\hat{\rho}_T$, the latter describing the closed, full system? This question is resolved by the reduced density operator. If the total system T consists of a subsystem S and an environment E , then the reduced density matrix for the subsystem is given by

$$\hat{\rho}_S = \text{Tr}_E(\hat{\rho}_T), \quad (2.5)$$

where Tr_E is the partial trace over the environment. The partial trace essentially takes the average with respect to the environmental degrees of freedom. This way, a

density operator for the subsystem of interest is obtained without having to simulate the whole system. The reduced density operator contains all measurement statistics of interest in the subsystem, placing it at the core of the theory of open quantum systems [8].

2.2.2 The Lindblad Master equation

An important framework for determining the dynamics of an open quantum system is the master equation approach. A classical master equation is defined by

$$\frac{dp_i}{dt} = \sum_j R_{ji}p_j - \sum_j R_{ij}p_i, \quad (2.6)$$

with probabilities p_i of being in state $|\psi_i\rangle$, and transition rates R_{ij} describing the rate of transitions from $|\psi_i\rangle$ to $|\psi_j\rangle$. As an example, the states in a quantum dot system may correspond to the number of electrons on the dot while the transition rates are typically related to the Fermi-Dirac distributions of the reservoirs and the tunneling rates of the barriers [19].

Adding the condition $\sum_i p_i = 1$, such that the total probability is unity, to the master equation results in a system of ordinary differential equations. This can be solved numerically using standard methods for first order differential equations, such as the Runge-Kutta method [22]. Once the probabilities $p_i(t)$ are obtained, the time evolution of the system can be calculated. Returning to the quantum dot example, the transient dynamics of the current can then be calculated by considering the amount of charge tunneling through the barriers at each point in time, which is directly related to the tunneling rates and probabilities $p_i(t)$ [19].

While a classical master equation may give accurate results for some quantum systems, it leaves out important physics. A quantum master equation generalizes the notion of a classical master equation in the following sense: The unknown in a quantum master equation does not only contain the probabilities p_i of being in a quantum state $|\psi_i\rangle$, but also the coherences. Hence, a quantum master equation involves the full density matrix while a classical master equation only includes the diagonal elements. As discussed previously, it is always possible to find a basis in which the density matrix is diagonal. However, this basis is in general not the eigenbasis of the Hamiltonian, and therefore does not represent classically physical states. Hence, a quantum master equation indeed generalizes its classical counterpart.

The starting point for quantum master equations is the von Neumann equation given by Eq. (2.4), for the density matrix of the total system. This equation is exact, but since the total system generally has a macroscopic amount of degrees of freedom, is not solvable. To progress, the idea is to reduce the number of degrees of freedom by applying the partial trace to trace out the environment, and then make suitable approximations to obtain a solvable quantum master equation for the smaller system of interest. A standard approximation is to assume that the coupling between the system and the environment is weak in comparison to the other energy scales of the system, such that the coupling can be treated perturbatively. This way, terms containing a coupling strength parameter of orders larger than a given precision can be neglected.

One of the most established quantum master equations is the so called Lindblad equation [23], which exists in several forms and can be derived in various ways.

In Ref. [20], a form of the Lindblad equation is derived directly from the microscopic dynamics. The first part of the derivation follows the steps described in the previous paragraph, i.e., considers the coupling perturbatively and traces out the environment. However, the resulting equation is in general still not solvable, and more approximations are necessary to proceed. One of the main assumptions that follows in the derivation is a Markovian approximation, meaning that the derivative of the density matrix is assumed to only depend on its current state, and not its past. At the end of the derivation, the following form of the Lindblad equation is obtained:

$$\frac{d\hat{\rho}}{dt} = i[\hat{\rho}, \hat{H}_{\text{eff}}] + \sum_i \hat{J}_i \hat{\rho} \hat{J}_i^\dagger - \frac{1}{2} \hat{\rho} \hat{J}_i^\dagger \hat{J}_i - \frac{1}{2} \hat{J}_i^\dagger \hat{J}_i \hat{\rho} \equiv \mathcal{L} \hat{\rho}, \quad (2.7)$$

where $\hat{\rho}$ is the reduced density operator, and \hat{H}_{eff} is the sum of two terms: the subsystem Hamiltonian \hat{H}_S and the Lamb shift Hamiltonian \hat{H}_{LS} . Originally, the Lamb shift was studied in atomic systems where the interaction with the quantum vacuum was found to cause a small shift of the energy levels. In open quantum systems, the Lamb shift Hamiltonian reflects a similar effect: a renormalization of energy levels due to the interaction with the environment [20]. The operators \hat{J}_i are the so called jump operators, which capture the coupling processes to the environment. In Ref. [24], a phenomenological approach for calculating the jump operators is described. Using this so called PERLind approach, each jump operator is associated with an actual, physical process. Taking a quantum dot system as an example, every jump operator then represents a certain tunneling event. Once the jump operators are constructed and the first term of Eq. (2.7) is calculated, an expression for the Liouvillian \mathcal{L} can be obtained.

The right hand side of the Lindblad equation can be divided into two parts. The first term, $i[\hat{\rho}, \hat{H}_{\text{eff}}]$, describes the unitary, free evolution of the system. A simple example of a free evolution would be the precession of magnetic moment in a magnetic field. The sum over i on the other hand, labeling, e.g., different tunneling events, correspond to the non-unitary and dissipative part of the dynamics [8]. The latter part causes the total Liouvillian to be non-Hermitian, which brings the possibility of EPs in the matrix representation of the Liouvillian.

2.3 Exceptional points

A matrix which describes the time evolution of a physical system, such as a Hamiltonian or a Liouvillian matrix, generally depends on the parameters of the system. These parameters span the so called parameter space, and it is in this space the EPs lie. An EP is defined as a point in the parameter space which causes two or more eigenvalues and their eigenvectors to simultaneously coalesce [2]. Furthermore, EPs can be of a different orders, reflecting how many eigenvectors coalesce at the point. The notion of EPs and its orders are directly related to a type of matrix decomposition, the Jordan normal form.

2.3.1 Jordan normal form

In physics, a common way to simplify calculations is to diagonalize the matrix generating the time evolution of the system. The diagonalization process can be

understood as a change of basis to linearly independent eigenvectors r_i , defined by $Ar_i = \lambda_i r_i$, where λ_i is the corresponding eigenvalue [25]. In this basis, the linear transformation of the matrix is very simple: it scales each eigenvector r_i by the corresponding eigenvalue. The matrix in the new basis is therefore diagonal, explaining the name of the process. For a matrix A and its diagonal form D , this can be written as

$$A = SDS^{-1}, \quad (2.8)$$

where $S = (r_1, \dots, r_n)$ consists of the eigenvectors of A .

However, not all matrices can be diagonalized, the exceptions being called defective matrices. For a defective matrix, there does not exist a complete basis of eigenvectors, and the diagonalization process is not possible [25]. This is closely related to the notion of EPs, since when two eigenvectors coalesce, one dimension is lost and the eigenvectors do not form a basis anymore. A matrix at an EP is therefore always defective.

Fortunately, there is a notion of an "almost diagonal" form for defective matrices, called the Jordan normal form. Recall that in the diagonalizable case, the basis is changed to the linearly independent eigenvectors. To construct the Jordan form for a defective matrix, this basis has to be completed in some way to span the full space. This can be done using Jordan chains [25], which for each eigenvector r_i with eigenvalue λ_i , consist of vectors $r_i, r_i^{(2)}, \dots, r_i^{(n_i)}$ defined by

$$\begin{aligned} (A - \lambda_i I)r_i &= 0, \\ (A - \lambda_i I)r_i^{(2)} &= r_i, \\ (A - \lambda_i I)r_i^{(3)} &= r_i^{(2)}, \\ &\vdots \\ (A - \lambda_i I)r_i^{(n_i)} &= r_i^{(n_i-1)}, \end{aligned} \quad (2.9)$$

where I is the identity matrix. The length of the i th chain, n_i , depends on the number of coalescing eigenvectors, and is therefore the same as the order of the corresponding EP. Note that for eigenvectors not involved in an EP, i.e., for eigenvectors which have not coalesced, the Jordan chain is of length one, only consisting of the eigenvectors themselves.

The vectors forming the Jordan chain are also known as the right generalized eigenvectors, which indicates the notion of *left* generalized eigenvectors. Regular left eigenvectors l_i are row vectors, defined by $l_i A = \lambda_i l_i$. These can then be extended to left generalized eigenvectors in a similar way as the right ones, forming Jordan chains $l_i, l_i^{(2)}, \dots, l_i^{(n_i)}$. The left generalized eigenvectors can be constructed such that $l_i^{(s)} r_j^{(t)} = \delta_{ij} \delta_{st}$, i.e, biorthogonally to the right generalized eigenvectors [2]. Creating these left and right Jordan chains for each linearly independent eigenvector results in q pairs of chains, each of which are collected into the matrices

$$\begin{aligned} \{\mathbf{r}_i\}_{i=1}^q, \text{ where } \mathbf{r}_i &= \begin{bmatrix} r_i & r_i^{(2)} & \dots & r_i^{(n_i)} \end{bmatrix}, \\ \{\mathbf{l}_i\}_{i=1}^q, \text{ where } \mathbf{l}_i &= \begin{bmatrix} l_i \\ l_i^{(2)} \\ \dots \\ l_i^{(n_i)} \end{bmatrix}. \end{aligned} \quad (2.10)$$

Here, the bold font in \mathbf{r}_i (\mathbf{l}_i) indicates a collection of column (row) vectors next to (below) each other, forming a matrix. The set of right generalized eigenvectors from all Jordan chains is called the canonical basis of the transformation. Using this new basis, the transformation matrix M can be formed:

$$M = [\mathbf{r}_1 \dots \mathbf{r}_q], \quad (2.11)$$

which also is known as the modal matrix. The inverse modal matrix M^{-1} , can be formed in terms of the left generalized eigenvectors:

$$M^{-1} = \begin{bmatrix} \mathbf{l}_1 \\ \vdots \\ \mathbf{l}_q \end{bmatrix}, \quad (2.12)$$

since $\mathbf{l}_j \mathbf{r}_i = \delta_{ij} I$ where I is the $n_j \times n_i$ identity matrix. This follows from the biorthogonality of the left and right generalized eigenvectors.

The Jordan normal form of A is then finally obtained by forming $J = M^{-1} A M$ and has the following structure:

$$J = \begin{bmatrix} J_{n_1}(\lambda_1) & \dots & 0 \\ \vdots & \ddots & \vdots \\ 0 & \dots & J_{n_q}(\lambda_q) \end{bmatrix}, \text{ where } J_{n_i}(\lambda_i) = \begin{bmatrix} \lambda_i & 1 & \dots & 0 \\ \vdots & \ddots & \ddots & \vdots \\ \vdots & & \ddots & 1 \\ 0 & \dots & \dots & \lambda_i \end{bmatrix}. \quad (2.13)$$

The Jordan form hence consists of q Jordan blocks $J_{n_i}(\lambda_i)$ on the diagonal, where each block is of size n_i and consists of its eigenvalue on the diagonal and ones on the super diagonal [25]. Note that if all blocks are of size one, i.e., if there are no EPs, the Jordan form is diagonal. The Jordan normal form can therefore be thought of a generalization of the diagonal form D .

Unfortunately, the Jordan form of a matrix is notoriously difficult to calculate numerically. This stems from the fact that an arbitrary small perturbation away from an EP completely changes the Jordan form. The process is therefore inherently numerically unstable [26]. For simple cases, it is however possible to work around this difficulty by introducing a small tolerance to determine if eigenvalues and their eigenvectors have coalesced. One can then infer the block structure of the Jordan form and construct it manually.

To be able to use the Jordan form in calculations, a substitution $A \rightarrow M J M^{-1}$ has to be made, and hence, the matrices M and M^{-1} are also desirable to compute numerically. These matrices consist of the right and left generalized eigenvectors, which can be calculated by the following process. Firstly, the regular eigenvectors are calculated by some numerical method, e.g., the `scipy.linalg.eig` function in Python. If there are coalesced eigenvectors (within the tolerance), the corresponding Jordan chains need then to be computed. This can be done by solving the defining equations for the generalized eigenvectors given by Eq. (2.9). However, since $A - \lambda_i I$ is not of full rank, the equations are underdetermined, meaning that there is no unique solution. A standard way of solving this problem is by using the Moore-Penrose pseudoinverse, which finds one of the solutions to the equation [25]. This process is then repeated until the full Jordan chains for each set of coalescing eigenvectors are calculated, obtaining all of the generalized eigenvectors. Finally, by biorthogonalizing the two sets of vectors, the modal matrix M and its inverse M^{-1} are obtained. Alternatively, M^{-1} can be calculated by numerically inverting M .

2.3.2 General solution of linear ODEs

A useful application of the Jordan form is for analytical solutions of ordinary differential equations (ODEs). A linear ODE is differential equation of the form

$$\frac{dx}{dt} = Ax. \quad (2.14)$$

Often, the unknown x is a vector, and A a matrix. The solution can then be written as a matrix exponential in the following way:

$$x(t) = e^{At}x(0), \text{ where } e^{At} = \sum_{k=0}^{\infty} \frac{(At)^k}{k!}. \quad (2.15)$$

The matrix exponential can be simplified using Jordan decomposition. In Ref. [25], it is shown that $e^{At} = Me^{Jt}M^{-1}$ where M is the modal matrix and

$$e^{Jt} = \begin{bmatrix} e^{J_{n_1}(\lambda_1)t} & \dots & 0 \\ \vdots & \ddots & \vdots \\ 0 & \dots & e^{J_{n_q}(\lambda_q)t} \end{bmatrix}, \text{ where } e^{J_{n_i}(\lambda_i)t} = e^{\lambda_i t} \begin{bmatrix} 1 & t & \dots & \frac{t^{n_i-1}}{(n_i-1)!} \\ \vdots & \ddots & \ddots & \vdots \\ \vdots & & \ddots & t \\ 0 & \dots & \dots & 1 \end{bmatrix}. \quad (2.16)$$

The matrix exponential therefore consists of entries with terms of the form $t^k e^{\lambda_i t}$ [25]. Note that if A is diagonalizable, all blocks are of size one and the entries consist of pure exponentials on the diagonal.

Using this result, the solution to Eq. (2.14) can be written as

$$x(t) = Me^{Jt}M^{-1}x(0). \quad (2.17)$$

This can further be decomposed if one considers the generalized modes of the system. A generalized mode in this context is meant as the solution to the ODE, with an initial condition in a linear combination of vectors in *one* of the Jordan chains. It can be shown that the trajectory then never leaves that Jordan chain throughout the whole time evolution.

To show this, suppose first that the initial state is in such an initial state, i.e., in a linear combination of vectors in one of the Jordan chains:

$$x(0) = a_1 r_i + a_2 r_i^{(2)} + \dots + a_{n_i} r_i^{(n_i)} = \mathbf{r}_i a, \quad (2.18)$$

where $a = (a_1, \dots, a_{n_i})^T$ is a constant vector and \mathbf{r}_i is defined in Eq. (2.11). Inserting this into Eq. (2.17), the solution can be written as

$$x(t) = Me^{Jt}M^{-1}x(0) = Me^{Jt} \begin{bmatrix} \mathbf{l}_1 \\ \vdots \\ \mathbf{l}_q \end{bmatrix} \mathbf{r}_i a = \mathbf{r}_i e^{J_{n_i}(\lambda_i)t} a. \quad (2.19)$$

Hence, the solution stays in the space spanned by the initial condition throughout the time evolution, as earlier proposed. For an arbitrary initial condition, the solution can be written as a sum over these generalized modes:

$$x(t) = \sum_{i=1}^q \mathbf{r}_i e^{J_{n_i}(\lambda_i)t} \mathbf{l}_i x(0), \quad (2.20)$$

and the initial condition therefore decides what modes are included in the dynamics of the system. A more detailed derivation of Eqs. (2.19) and (2.20) is done in Appendix A.

Translating this theory into the language of Liouvillian physics, the underlying ODE is given by the Lindblad equation, transformed to Fock-Liouville space

$$\frac{d\rho(t)}{dt} = \mathcal{L}\rho(t) \rightarrow \frac{d}{dt} |\rho(t)\rangle\rangle = L |\rho(t)\rangle\rangle, \quad (2.21)$$

where L is the matrix representation of the Liouvillian and $|\rho(t)\rangle\rangle$ the vectorized density matrix. Using Eq. (2.20), the solution can then be written in terms of the eigenvalues and generalized eigenvectors of L .

Chapter 3

Results: EP-dynamics in a parallel dot system

Equipped with the necessary theory, the dynamics of the parallel QD system can now be simulated. The equation of motion for the system is the Lindblad equation, given by Eq. (2.7), for the reduced density operator of the two quantum dots. In Fock-Liouville space, the Lindblad equation is given by Eq. (2.21), with a matrix representation of the Liouvillian, L . Specifying the values of the parameters of the system, L can be constructed from the jump operators and the effective Hamiltonian in the Lindblad equation. By then searching for coalescing eigenvalues and eigenvectors of L in the parameter space, EPs can be located, at which the dynamics obey Eq. (2.20). Finally, Eq. (2.3) can be used to simulate the transient current through the parallel QD system. The numerical calculations were done in Python using standard tools from the `numpy` and `scipy` packages. Furthermore, a piece of code which already implemented the PERLind approach for calculating the jump operators and the rest of the Liouvillian was used as a starting point for further calculations. Both this pre-existing code and the code developed during the work of the thesis can be found in Ref. [27].

3.1 Model

In this thesis, a particular quantum dot system was studied, consisting of two quantum dots connected to two leads, both of them in thermal equilibrium. Similarly to the works in e.g. Refs. [18, 28], the quantum dots are assumed to be coupled in parallel to the leads, meaning that the dots are coupled to the same lead on each side. For simplicity, the electrons are assumed to be spinless, which is a good approximation for a low bias voltage in the presence of a magnetic field. However, the bias voltage considered in this thesis is cannot be considered to be small, and hence we must rely on an assumption of the system only containing one spin species. Furthermore, it is assumed that there is no direct tunneling between the dots. However, we consider an interacting system, with a finite contribution from the Coulomb repulsion between the electrons in the case of double occupancy. A sketch of the model is given in Fig. 3.1.

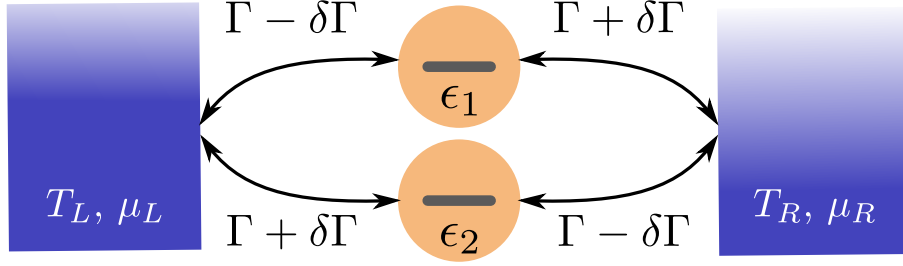


Figure 3.1: The modeled parallel dot system, where the quantum dots in the center have energies ϵ_1 and ϵ_2 . Located on the sides are the two reservoirs R, L with temperatures $T_{L/R}$ and chemical potentials $\mu_{L/R}$. The allowed tunneling processes are indicated with arrows, with corresponding tunneling rates $\Gamma \pm \delta\Gamma$.

To reduce the dimension of the parameter space, a fixed tunneling rate Γ and a variable tunneling detuning $\delta\Gamma$ are introduced. The four tunneling rates in terms of Γ and $\delta\Gamma$ are assumed to be asymmetric, as indicated by Fig. 3.1. It is also assumed that each dot is restricted to be either empty or contain one (spinless) electron. The energy levels of the two QDs are assumed to be given by $\epsilon_{1/2} = -V_G \pm \delta\epsilon$, with a variable energy detuning $\delta\epsilon$ and a gate voltage V_G , which we set to zero. Furthermore, the temperatures of the leads $T_L = T_R = 10\Gamma$, the chemical potentials $\mu_{L/R} = \pm V_{SD}/2$, the bias voltage $V_{SD} = 300\Gamma$, and the Coulomb energy $U = 250\Gamma$, are all fixed in terms of Γ . This leaves the two tuning parameters, $\delta\Gamma$ and $\delta\epsilon$, as the only parameters of the system, resulting in a two dimensional parameter space.

To be able to justify the Lindblad approach for calculating the dynamics of the system, one more major approximation has to be made regarding the coupling between the dots and the leads. We must assume that the strength of the coupling between the system and the environment is weak in comparison with the temperature, i.e., $\Gamma \ll T$. In this so called weak-coupling limit, the Lindblad equation is a standard approach for investigating the dynamics of a quantum dot system. In this thesis, we consider terms up to first order in Γ . This approximation neglects effects such as cotunneling, where several electrons simultaneously tunnel into and out of the QDs [18]. Hence, we only consider sequential tunneling processes.

The total system can be modeled by the Hamiltonian

$$\hat{H} = \hat{H}_{\text{QD}} + \hat{H}_{\text{leads}} + \hat{H}_{\text{tunneling}}, \quad (3.1)$$

where the three terms correspond to the quantum dot, lead, and tunneling Hamiltonians

$$\begin{aligned} \hat{H}_{\text{QD}} &= \sum_{i=1,2} \epsilon_i \hat{d}_i^\dagger \hat{d}_i + U \hat{d}_1^\dagger \hat{d}_1 \hat{d}_2^\dagger \hat{d}_2, \\ \hat{H}_{\text{leads}} &= \sum_{k,s=L,R} E_{s,k} \hat{c}_{s,k}^\dagger \hat{c}_{s,k}, \\ \hat{H}_{\text{tunneling}} &= \sum_{i=1,2} \sum_{k,s=L,R} t_{s,i} \hat{c}_{s,k}^\dagger \hat{d}_i + t_{s,i}^* \hat{d}_i^\dagger \hat{c}_{s,k}, \end{aligned} \quad (3.2)$$

where \hat{d}_i^\dagger (\hat{d}_i), $i \in \{1, 2\}$, creates (annihilates) an electron in dot 1 or 2, and $\hat{c}_{l,k}^\dagger$ ($\hat{c}_{l,k}$), $s \in \{L, R\}$, creates (annihilates) an electron in the left (L) or right (R) lead with momentum k and energy $E_{s,k}$ [18]. The tunneling amplitudes $t_{s,i}$ are directly related

to the corresponding tunneling rates by

$$\Gamma_{s,i} = 2\pi\nu_F |t_{s,i}|^2, \quad (3.3)$$

where ν_F is the density of states in the lead, which we assume to be independent of energy [24].

To represent the operators in matrix form, the many-body eigenstates of the isolated quantum dot Hamiltonian are used as the basis:

$$\begin{aligned} |a\rangle &= |00\rangle \\ |b\rangle &= |10\rangle = \hat{d}_1^\dagger |00\rangle \\ |c\rangle &= |01\rangle = \hat{d}_2^\dagger |00\rangle \\ |d\rangle &= |11\rangle = \hat{d}_1^\dagger \hat{d}_2^\dagger |00\rangle, \end{aligned} \quad (3.4)$$

where n_1 and n_2 in $|n_1 n_2\rangle$ are the number of electrons in the first and second QD, respectively. The quantum dot and tunneling Hamiltonians are in this basis given by

$$\begin{aligned} \hat{H}_{\text{QD}} &= \epsilon_1 |b\rangle \langle b| + \epsilon_2 |c\rangle \langle c| + (\epsilon_1 + \epsilon_2 + U) |d\rangle \langle d| \\ \hat{H}_{\text{tunneling}} &= \sum_{k,s=L,R} [t_{s,1}^* (|b\rangle \langle a| + |d\rangle \langle c|) + t_{s,2}^* (|c\rangle \langle a| - |d\rangle \langle b|)] \hat{c}_{s,k} + \text{H.c.}, \end{aligned} \quad (3.5)$$

where the minus sign in the second term in the tunneling Hamiltonian comes from the fact that $d_2^\dagger d_1^\dagger = -d_1^\dagger d_2^\dagger$ for fermions.

In the basis given by Eq. (3.4), the elements of the reduced density matrix can be written as $\rho_{\alpha\beta}$, where $\alpha, \beta \in \{a, b, c, d\}$, with 16 matrix elements. However, the only non-zero off-diagonal elements are ρ_{bc} and ρ_{cb} , i.e, the elements which corresponds to superpositions of the two states with one occupied dot. This is the result of charge being a conserved quantity in the total system. The number of elements in $|\rho\rangle\rangle$ is therefore reduced to six, which in turn means that the Liouvillian effectively can be represented by a 6×6 matrix. The vectorization of the density matrix can be done in several ways, but in this thesis it is given by

$$\rho = \begin{bmatrix} \rho_{aa} & 0 & 0 & 0 \\ 0 & \rho_{bb} & \rho_{bc} & 0 \\ 0 & \rho_{cb} & \rho_{cc} & 0 \\ 0 & 0 & 0 & \rho_{dd} \end{bmatrix} \rightarrow |\rho\rangle\rangle = \begin{bmatrix} \rho_{aa} \\ \rho_{bb} \\ \rho_{cc} \\ \rho_{dd} \\ \text{Re } \rho_{bc} \\ \text{Im } \rho_{bc} \end{bmatrix}. \quad (3.6)$$

Since the density matrix is Hermitian, the diagonal elements are real and $\rho_{bc} = \rho_{cb}^*$. Hence, for the off-diagonal elements, it is enough to specify $\text{Re } \rho_{bc}$ and $\text{Im } \rho_{bc}$ to obtain an equivalent vectorized representation of the density matrix.

3.2 Spectrum

The first step towards simulating the dynamics of the parallel dot system was to calculate the matrix representation of the Liouvillian. This was obtained from the

code implementing the PERLind approach mentioned the beginning of this chapter. The code calculates the four jump operators, one for each tunneling process, and then constructs the unitary part of Eq. (2.7). Finally, the code puts these two pieces together, resulting in the Liouvillian matrix L . We then compared the result with calculations from the Python-based QmeQ package [29] for comparison. The basis and ordering used for L and $|\rho\rangle\rangle$ is given by Eqs. (3.4) and (3.6). Once the Liouvillian was obtained, the parameter space was searched for EPs by numerically calculating the eigenvalues of L for varying $\delta\epsilon$ and $\delta\Gamma$. A degeneracy of eigenvalues was found at $\lambda_5 = \lambda_6 \approx -0.5\Gamma$, for $\delta\Gamma = 10^{-6}\Gamma$ and $\delta\epsilon \approx 0.3\Gamma$, see Fig. 3.2. The corresponding eigenvectors, $|\rho_5\rangle\rangle$ and $|\rho_6\rangle\rangle$, were found to also coalesce, confirming the existence of a second order EP. The eigenvalue and right eigenvector corresponding to the EP will be denoted by $\bar{\lambda}$ and $|\bar{\rho}\rangle\rangle$, respectively.

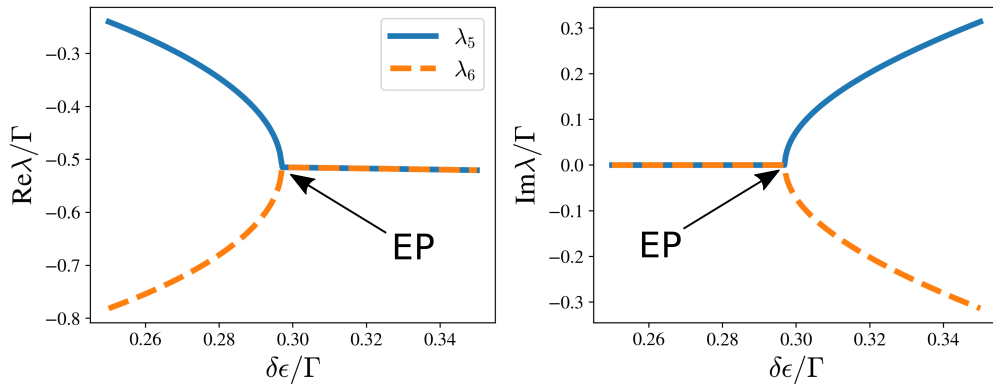


Figure 3.2: The real and imaginary part of two eigenvalues to L , λ_5 and λ_6 , for varying $\delta\epsilon$. An eigenvalue degeneracy can be seen at $\delta\epsilon \approx 0.3\Gamma$.

The full spectrum of the Liouvillian at the EP is given in Fig. 3.3, where the eigenvalue degeneracy between λ_5 and λ_6 is clear. There is almost a degeneracy between λ_3 and λ_4 , however, this is not a second EP since the eigenvectors are not parallel. Furthermore, note that all $\lambda_{i>1}$ are on the negative real axis, indicating non-oscillatory, exponential decay towards the steady-state in the dynamics of the system. This steady-state is given by the eigenvector corresponding to the zero eigenvalue λ_1 , since then $\frac{d}{dt} |\rho_1\rangle\rangle = 0$.

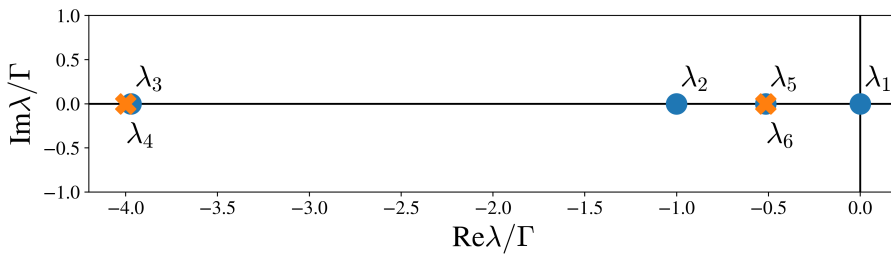


Figure 3.3: The spectrum of the Liouvillian at the EP, where the degeneracy between λ_5 and λ_6 is the relevant one. The crosses are used to distinguish eigenvalues which are close to each other.

3.3 Dynamics

Using Eq. (2.20), the time evolution of the system can be given in terms of the eigenvalues and generalized eigenvectors of L . Away from an EP, the Liouvillian is diagonalizable, and the terms are purely exponential. The time evolution of the density operator is then given by

$$|\rho(t)\rangle\rangle = |\rho_{ss}\rangle\rangle + \sum_{i=2}^6 c_i e^{\lambda_i t} |\rho_i\rangle\rangle, \quad (3.7)$$

where $|\rho_i\rangle\rangle$ is the i th right eigenvector of L , and $c_i = \langle\langle\sigma_i|\rho(0)\rangle\rangle$. Here, $\langle\langle\sigma_i|$ is the i th left eigenvector, constructed biorthogonally to $|\rho_i\rangle\rangle$ such that $\langle\langle\sigma_i|\rho_j\rangle\rangle = \delta_{ij}$, and $|\rho_{ss}\rangle\rangle = c_1 |\rho_1\rangle\rangle$ is the steady-state of the system. Furthermore, $|\rho_{ss}\rangle\rangle$ is the only eigenvector for which the first four elements add up to one, i.e., the only eigenvector which represents a density matrix with unity trace, see Eq. (3.6). This implies that the rest of the other eigenvectors must be traceless for $|\rho\rangle\rangle$ to have unity trace. Hence, the eigenvectors $|\rho_{i>1}\rangle\rangle$, do not describe physical states on their own.

At the EP, the Jordan form of L and its exponential, $\exp(Jt)$, have to be evaluated. Since the EP is of order two, this results in a 2×2 Jordan block. This is the only EP, which means that rest of the Jordan form is diagonal. Using Eqs. (2.13) and (2.16), this results in the following Jordan form and Jordan exponential:

$$J = \begin{bmatrix} 0 & 0 & 0 & 0 & 0 & 0 \\ 0 & \lambda_2 & 0 & 0 & 0 & 0 \\ 0 & 0 & \lambda_3 & 0 & 0 & 0 \\ 0 & 0 & 0 & \lambda_4 & 0 & 0 \\ 0 & 0 & 0 & 0 & \bar{\lambda} & 1 \\ 0 & 0 & 0 & 0 & 0 & \bar{\lambda} \end{bmatrix}, \quad e^{Jt} = \begin{bmatrix} 1 & 0 & 0 & 0 & 0 & 0 \\ 0 & e^{\lambda_2 t} & 0 & 0 & 0 & 0 \\ 0 & 0 & e^{\lambda_3 t} & 0 & 0 & 0 \\ 0 & 0 & 0 & e^{\lambda_4 t} & 0 & 0 \\ 0 & 0 & 0 & 0 & e^{\bar{\lambda} t} & t \\ 0 & 0 & 0 & 0 & 0 & e^{\bar{\lambda} t} \end{bmatrix}, \quad (3.8)$$

since $\lambda_1 = 0$.

Furthermore, the Jordan chain vector, here written as $|\rho'\rangle\rangle$, defined by

$$(L - \bar{\lambda}I) |\rho'\rangle\rangle = |\bar{\rho}\rangle\rangle, \quad (3.9)$$

and the left generalized eigenvectors $\langle\langle\sigma'|$ and $\langle\langle\bar{\sigma}|$, need to be evaluated. The left generalized eigenvectors are constructed such that $\langle\langle\sigma'|\rho'\rangle\rangle = \langle\langle\bar{\sigma}|\bar{\rho}\rangle\rangle = 1$, and orthogonal to all other right generalized eigenvectors. Inserting these vectors into Eq. (2.20) leads, after a bit of work, to

$$|\rho(t)\rangle\rangle = |\rho_{ss}\rangle\rangle + \sum_{i=2}^4 c_i e^{\lambda_i t} |\rho_i\rangle\rangle + (\bar{c} + c't) e^{\bar{\lambda} t} |\bar{\rho}\rangle\rangle + c' e^{\bar{\lambda} t} |\rho'\rangle\rangle, \quad (3.10)$$

where $\bar{c} = \langle\langle\bar{\sigma}|\rho(0)\rangle\rangle$, and $c' = \langle\langle\sigma'|\rho(0)\rangle\rangle$.

By numerically calculating the generalized eigenvectors as described in Section 2.3.1, the dynamics at and away from the EP, given by Eqs. (3.7) and (3.10), were implemented. The results were then compared with a numerical ODE-solver. The numerical solver was set to an absolute and relative tolerance of 10^{-10} and 10^{-6} respectively. The relative difference from the implemented methods to the numerical solver, given by $\|\rho(t) - \rho_{\text{num}}(t)\|_1 / \|\rho_{\text{num}}(t)\|_1$, was in the order of 10^{-8} at all

times, at and away from the EP. Here, $\|\cdot\|_1$ represents the matrix 1-norm, i.e. the maximum absolute column sum of the matrix. With the use of strict tolerances of the numerical solver, the small relative difference indicates an accurate method. Furthermore, when reducing the tolerances even more, the distance kept lowering, indicating that the numerical solver might be the limiting factor. It is hence clear that the implemented methods produce an accurate result at and away from the EP.

3.3.1 Varying initial conditions

With a clear picture of the analytical dynamics and numerically calculated eigenvalues and generalized eigenvectors at hand, simulations of the parallel dot system were performed. Firstly, the time evolution in the generalized modes was investigated. This was done by introducing initial conditions consisting of linear combinations of the generalized eigenvectors

$$|\rho(0)\rangle\rangle = |\rho_{ss}\rangle\rangle + \sum_{i=2}^4 b_i |\rho_i\rangle\rangle + \bar{b} |\bar{\rho}\rangle\rangle + b' |\rho'\rangle\rangle. \quad (3.11)$$

This way, the constants c in Eq. (3.10) are the same as the corresponding constants labeled with b in Eq. (3.11). The generalized modes included in the time evolution can then be controlled by the initial condition. To see this, simulations of the density matrix for different initial conditions were done and then compared with the steady-state of the system, see Fig. 3.4a.

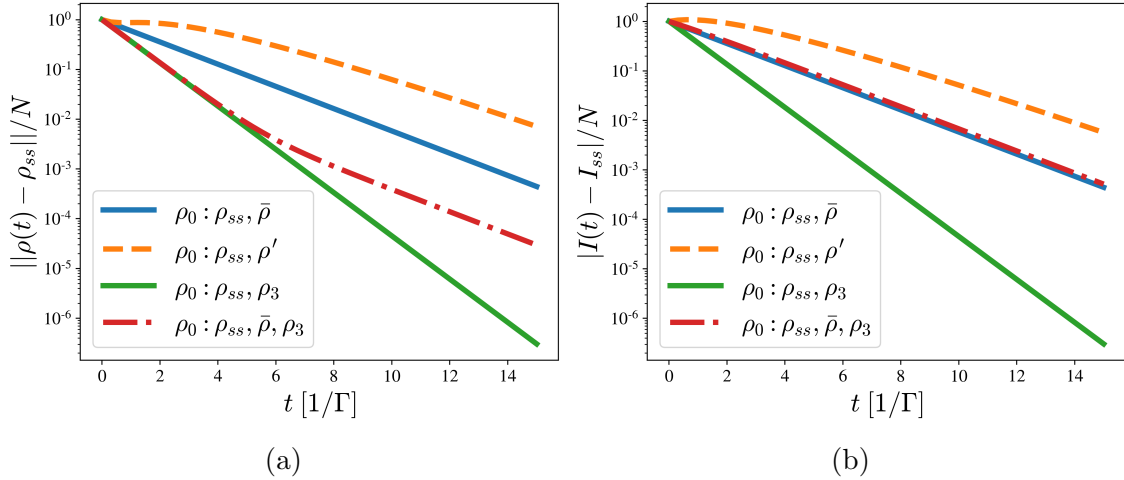


Figure 3.4: The decay of the density matrix (a) and the current (b), towards the steady-state density matrix ρ_{ss} and current I_{ss} in a logarithmic plot. The simulations were done at the EP with different initial conditions in linear combinations of the generalized eigenvectors, see Eq. (3.11). The linear combinations used for the initial conditions are given by the following: the solid, blue line: $\bar{b} = 1$, the dashed, yellow line: $b' = 1$, the solid, green line: $b_3 = 1$, and the dash-dotted, red line: $\bar{b} = 1$, $b_3 = 15$, all other constants being zero if not mentioned. A normalization by $N = \|\rho(0) - \rho_{ss}\|$ and $N = |I(0) - I_{ss}|$ was done such that each curve is unity for $t = 0$. Here, $\|\cdot\|$ represents the Euclidean norm of the vectorized density matrices.

With initial conditions including only one $b_i \neq 0$ or $\bar{b} \neq 0$, i.e., only one normal eigenvector excluding $|\rho_{ss}\rangle\rangle$, a mode consisting of pure exponential decay toward the

steady-state is seen by the straight lines in the logarithmic plot. This is expected since the time evolution only picks up one of the exponentials from Eq. (3.10). The quicker decay corresponds to $|\rho_3\rangle\rangle$ since $|\lambda_3| > |\bar{\lambda}|$, see Fig. 3.3. When including both $|\bar{\rho}\rangle\rangle$ and $|\rho_3\rangle\rangle$ in the initial condition, the decay first follows the quicker decay channel, then gradually turns into following the decay of $|\bar{\rho}\rangle\rangle$. Another behavior is seen for the initial condition including $|\rho'\rangle\rangle$. This generalized mode is not of exponential nature, since a factor of $t \exp(\bar{\lambda}t)$ enters in the dynamics. Away from an EP, the dynamics is given by Eq. (3.7) and this type of algebraic decay never happens. Thus, the behavior of this decay channel is a unique feature of the EP dynamics.

As discussed in Chapter 2, any relevant observable of the system can be obtained from the density operator. For the parallel dot system, the main observable is the current entering or leaving a lead, which by using Eq. (2.3) can be obtained by

$$\langle \hat{I}_s \rangle (t) = \text{Tr}(\hat{\rho}(t)\hat{I}_s), \quad (3.12)$$

with a current operator \hat{I}_s , corresponding to the current out of lead $s \in \{L,R\}$. The current operators can be phrased in terms of the jump operators from the Lindblad equation as

$$\hat{I}_s = \hat{J}_{s+}^\dagger \hat{J}_{s+} - \hat{J}_{s-}^\dagger \hat{J}_{s-}, \quad (3.13)$$

where $\hat{J}_{s\alpha}$, $\alpha \in \{+, -\}$, is the jump operator corresponding to tunneling events entering (+) a dot from lead s or leaving (-) a dot to lead s .

By calculating and collecting the jump operators using the aforementioned code implementing the PERLind approach and then inserting Eq. (3.13) into Eq. (3.12), the current through the QD system could be simulated. In Fig. 3.4b, the calculations from Fig. 3.4a were used to also simulate the current for the same initial conditions. The results are similar to the simulations of the density matrix, indicating that the time evolution in generalized modes carry over to the transient current dynamics. However, with the initial condition including the two normal eigenvectors, the decay in the quicker decay channel is washed out in this time scale and seemingly only follows the slower decay rate. This can be contrasted with the algebraic decay, which is equally visible in the current dynamics as in the density matrix dynamics.

3.3.2 Varying parameters

Simulations were also done to investigate the general behavior of the current at and slightly away from the EP. This is done in Fig. 3.5, for two different initial conditions: one with empty dots, and the other in a mixed state. These initial vectorized density matrices are given by

$$\begin{aligned} 1 : |\rho(0)\rangle\rangle &= |\rho_{\text{empty}}\rangle\rangle = [1 \ 0 \ 0 \ 0 \ 0 \ 0]^T \\ 2 : |\rho(0)\rangle\rangle &= |\rho_{\text{mixed}}\rangle\rangle = \frac{1}{4} [1 \ 1 \ 1 \ 1 \ 0 \ 0]^T. \end{aligned} \quad (3.14)$$

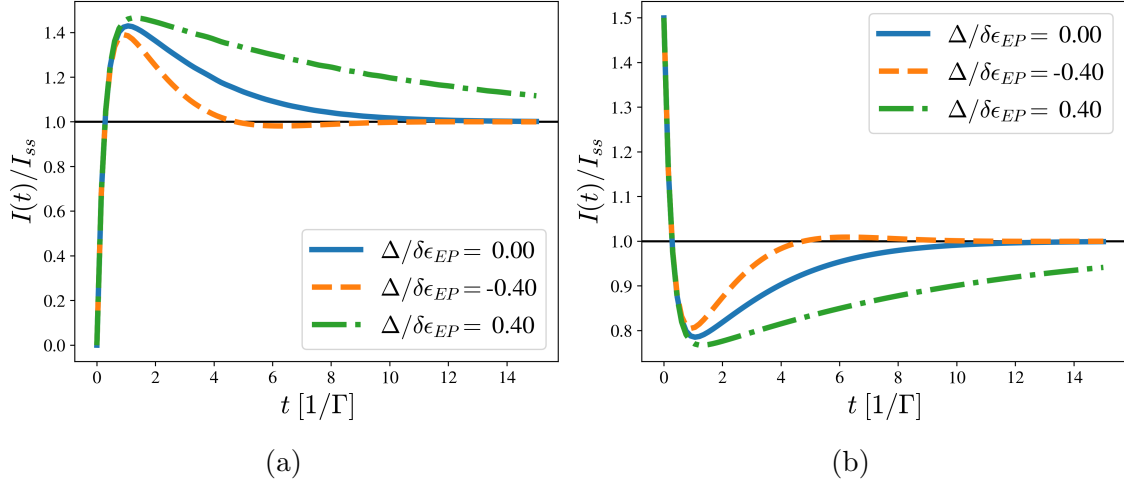


Figure 3.5: The current over time for different $\Delta = \delta\epsilon_{EP} - \delta\epsilon$, normalized by the corresponding steady-state current I_{ss} . The solid, blue curves correspond to the system being at the EP, while the other two are slightly away from it. The initial conditions are given by Eq. (3.14), with a) having the empty initial condition and b) the mixed one.

Looking at Fig. 3.5, it is clear that the three curves behave differently after the first phase of overshooting the steady-state, i.e., after $t \approx 2$. The curves corresponding to a $\Delta < 0$, slightly overshoot the steady-state once more before approaching the steady-state solution. This can be phrased as an underdamped behavior. On the other hand, for $\Delta > 0$, the decay towards the steady-state is very slow, which can be thought of as an overdamped system. Lastly, for the system at the EP, the decay is much faster than for the overdamped system, but does not overshoot the steady-state again like the underdamped system. This behavior is similar to what was found in Ref. [11] for quantum thermal machines, where the dynamics at the EP corresponded to the quickest decay without overshooting the steady-state, which is known as critical damping. Furthermore, it can be noted that the current dynamics in Fig. 3.5 varies continuously when approaching and leaving the EP, even though the notion of EPs at first sight does seem to invoke abrupt changes.

Chapter 4

Conclusion and outlook

Summarizing the results of the thesis, a second order EP in the Liouvillian generating the dynamics in a parallel dot system was demonstrated. After finding the EP, Jordan decomposition was used to understand the time evolution of the system in terms of the generalized modes, given by Eq. (3.10). Intuitively, this means that the Jordan chains, consisting of generalized eigenvectors, evolve separately, and that the initial density matrix decides which modes are involved in the dynamics of the system. Equation (3.10) also implies that the dynamics at the EP for certain initial conditions includes algebraic decay, as opposed to pure exponential decay away from the EP. It was also shown that these characteristics of the density operator carry over to the current through the system. Furthermore, comparisons of the transient current at and away from the EP indicated similarities to Ref. [11] regarding critical damping at the EP, but for a system of quantum dots instead of a quantum thermal machine.

From a computational point of view, one may argue that the dynamics could just as well have been simulated by a standard numerical integrator instead of the implemented methods in this thesis. However, the latter gives direct access to the generalized eigenvectors, which then could be used as initial conditions, directly controlling which modes to be included in the time evolution. This increased the understanding of the dynamics of the system and might prove useful for probing the system for interesting and useful dynamics. It is also important to note that the generalized eigenvectors were calculated through numerical means, which in theory can be done for even larger systems and higher order EPs, unlike algebraic methods.

One of the main applications discussed in the literature on EPs is sensing technologies [4–7]. As mentioned in the introduction, this is because eigenvalue splittings are more sensitive to small perturbations at an EP. In the framework of non-Hermitian physics, the eigenvalues of the operator in question, the Hamiltonian, are the energies of the system and hence directly observable. In Liouvillian physics, the eigenvalues instead correspond to the decay rates, which are more abstract and difficult to measure. An interesting open problem would be to find a useful observable that probes decay rates, such that similar sensing ideas could be applied to QDs and Liouvillian systems in general. Another proposed application for EPs is in quantum control, i.e., for steering a quantum system to a target state in an optimal way. The signs of critical decay at the EP in the parallel dot system are an indication of the validity of this application in systems of QDs. If the parallel dot system would act as a component in a bigger system, it may be important for it to reach its steady-state

with critical damping. If so, EPs in quantum dot systems may serve as a piece in the puzzle of reaching optimal performance in future technologies.

To conclude, considering the sparse amount of literature regarding EPs in Liouvillian systems, and in particular systems involving QDs, it is interesting that a system of quantum dots indeed can give rise to EPs. This opens up many questions of how to understand and exploit EPs in QD systems in the future. This thesis begins to answer these questions, and will hopefully lead to further work in the, so far, small world of exceptional points in quantum dots.

Bibliography

- ¹J. J. Sakurai and J. Napolitano, *Modern quantum mechanics*, 3rd ed. (Cambridge University Press, 2020).
- ²Y. Ashida, Z. Gong, and M. Ueda, “Non-hermitian physics”, *Advances in Physics* **69**, 249–435 (2020).
- ³W. D. Heiss, “Exceptional points of non-hermitian operators”, *Journal of Physics A: Mathematical and General* **37**, 2455–2464 (2004).
- ⁴M.-A. Miri and A. Alù, “Exceptional points in optics and photonics”, *Science* **363**, eaar7709 (2019).
- ⁵S. Ozdemir, S. Rotter, F. Nori, and L. Yang, “Parity–time symmetry and exceptional points in photonics”, *Nature Materials* **18**, 1 (2019).
- ⁶H. Hodaei, A. Hassan, S. Wittek, H. Garcia-Gracia, R. El-Ganainy, D. Christodoulides, and M. Khajavikhan, “Enhanced sensitivity at higher-order exceptional points”, *Nature* **548**, 187–191 (2017).
- ⁷W. Chen, Ş. Kaya Özdemir, G. Zhao, J. Wiersig, and L. Yang, “Exceptional points enhance sensing in an optical microcavity”, *Nature* **548**, 192–196 (2017).
- ⁸G. Schaller, *Open quantum systems far from equilibrium*, Vol. 881, Lecture Notes in Physics (2014).
- ⁹F. Roccati, G. M. Palma, F. Ciccarello, and F. Bagarello, “Non-hermitian physics and master equations”, *Open Systems & Information Dynamics* **29**, 10.1142/s1230161222500044 (2022).
- ¹⁰F. Minganti, A. Miranowicz, R. W. Chhajlany, and F. Nori, “Quantum exceptional points of non-hermitian hamiltonians and liouvillians: the effects of quantum jumps”, *Phys. Rev. A* **100**, 062131 (2019).
- ¹¹S. Khandelwal, N. Brunner, and G. Haack, “Signatures of Liouvillian exceptional points in a quantum thermal machine”, *PRX Quantum* **2**, 040346 (2021).
- ¹²P. Kumar, K. Snizhko, Y. Gefen, and B. Rosenow, “Optimized steering: quantum state engineering and exceptional points”, *Phys. Rev. A* **105**, L010203 (2022).
- ¹³S. A. Gurvitz and Y. S. Prager, “Microscopic derivation of rate equations for quantum transport”, *Phys. Rev. B* **53**, 15932–15943 (1996).
- ¹⁴L. Kouwenhoven and C. Marcus, “Quantum dots”, *Physics World* **11**, 35–40 (1998).
- ¹⁵L. P. Kouwenhoven, C. M. Marcus, P. L. McEuen, S. Tarucha, R. M. Westervelt, and N. S. Wingreen, “Electron transport in quantum dots”, in *Mesoscopic electron transport*, edited by L. L. Sohn, L. P. Kouwenhoven, and G. Schön (Springer Netherlands, Dordrecht, 1997), pp. 105–214.

- ¹⁶Dorsch, Sven, “Transport in nanowire-based quantum dot systems: Heating electrons and confining holes”, eng, PhD thesis (Lund University, 2022).
- ¹⁷F. P. G. de Arquer, D. V. Talapin, V. I. Klimov, Y. Arakawa, M. Bayer, and E. H. Sargent, “Semiconductor quantum dots: technological progress and future challenges”, *Science* **373**, eaaz8541 (2021).
- ¹⁸Z.-Z. Li and M. Leijnse, “Quantum interference in transport through almost symmetric double quantum dots”, *Phys. Rev. B* **99**, 125406 (2019).
- ¹⁹R. A. Bush, E. D. Ochoa, and J. K. Perron, “Transport through quantum dots: An introduction via master equation simulations”, *American Journal of Physics* **89**, 300–306 (2021).
- ²⁰D. Manzano, “A short introduction to the Lindblad master equation”, *AIP Advances* **10**, 025106 (2020).
- ²¹H. Bruus and K. Flensberg, *Many-body quantum theory in condensed matter physics: an introduction*, Oxford Graduate Texts (OUP Oxford, 2004).
- ²²A. Iserles, *A first course in the numerical analysis of differential equations* (Cambridge University Press, 2009).
- ²³G. Lindblad, “On the generators of quantum dynamical semigroups”, *Communications in Mathematical Physics* **48**, 119–130 (1976).
- ²⁴G. Kiršanskas, M. Franckić, and A. Wacker, “Phenomenological position and energy resolving lindblad approach to quantum kinetics”, *Phys. Rev. B* **97**, 035432 (2018).
- ²⁵A. Holst and V. Ufnarovski, *Matrix theory* (Studentlitteratur, 2014).
- ²⁶R. A. Horn and C. R. Johnson, *Matrix analysis* (Cambridge University Press, 1985).
- ²⁷W. Samuelson, “*bsc-thesis*”, <https://github.com/williamesamuelson/bsc-thesis>, [Online, GitHub], 2022.
- ²⁸M. A. Sierra, M. Saiz-Bretin, F. Dominguez-Adame, and D. Sanchez, “Interactions and thermoelectric effects in a parallel-coupled double quantum dot”, *Phys. Rev. B* **93**, 235452 (2016).
- ²⁹G. Kiršanskas, J. N. Pedersen, O. Karlström, M. Leijnse, and A. Wacker, “QmeQ 1.0: an open-source Python package for calculations of transport through quantum dot devices”, *Computer Physics Communications* **221**, 317–342 (2017).

Appendix A

Derivation of Equation (2.20)

Here, we consider a general linear ODE of the form $\dot{x} = Ax$ and derive the solution in terms of generalized modes given by Eq. (2.20). First, we follow the steps in the main text by introducing an initial condition contained in one of the Jordan chains:

$$x(0) = a_1 r_i + a_2 r_i^{(2)} + \dots + a_{n_i} r_i^{(n_i)} = \mathbf{r}_i a, \quad (\text{A.1})$$

where $a = (a_1, \dots, a_{n_i})^T$ is a constant vector and \mathbf{r}_i is defined in Eq. (2.11). Inserting this into Eq. (2.17) gives

$$x(t) = M e^{Jt} M^{-1} x(0) = M e^{Jt} \begin{bmatrix} \mathbf{l}_1 \\ \vdots \\ \mathbf{l}_q \end{bmatrix} \mathbf{r}_i a = M e^{Jt} \begin{bmatrix} 0_{n_1 \times n_i} \\ \vdots \\ I_{n_i \times n_i} \\ \vdots \\ 0_{n_q \times n_i} \end{bmatrix} a, \quad (\text{A.2})$$

where the last step follows from that each product $\mathbf{l}_j \mathbf{r}_i$ results in $n_j \times n_i$ blocks of zeros if $j \neq i$ and the $n_i \times n_i$ identity matrix if $i = j$. Inserting the Jordan exponential now gives

$$\begin{aligned} x(t) &= M \begin{bmatrix} e^{J_{n_1}(\lambda_1)t} & \dots & 0 \\ \vdots & \ddots & \vdots \\ 0 & \dots & e^{J_{n_q}(\lambda_q)t} \end{bmatrix} \begin{bmatrix} 0_{n_1 \times n_i} \\ \vdots \\ I_{n_i \times n_i} \\ \vdots \\ 0_{n_q \times n_i} \end{bmatrix} a = [\mathbf{r}_1 \dots \mathbf{r}_q] \begin{bmatrix} 0_{n_1 \times n_i} \\ \vdots \\ e^{J_{n_i}(\lambda_i)t} \\ \vdots \\ 0_{n_q \times n_i} \end{bmatrix} a = \\ &= \mathbf{r}_i e^{J_{n_i}(\lambda_i)t} a. \end{aligned} \quad (\text{A.3})$$

We can write a general initial condition as a linear combination of vectors in all Jordan chains as follows:

$$x(0) = \sum_{i=1}^q \mathbf{r}_i a^{(i)}, \quad (\text{A.4})$$

where each $a^{(i)}$ is a constant vector, similarly to Eq. (A.1), for each Jordan chain. Inserting this initial condition into Eq. (2.17), and using Eqs. (A.2) and (A.3) results

in

$$\begin{aligned} x(t) &= Me^{Jt}M^{-1}x(0) = Me^{Jt}M^{-1}\sum_{i=1}^q \mathbf{r}_i a^{(i)} = \sum_{i=1}^q Me^{Jt}M^{-1}\mathbf{r}_i a^{(i)} = \\ &= \sum_{i=1}^q \mathbf{r}_i e^{J_{n_i}(\lambda_i)t} a^{(i)} = \sum_{i=1}^q \mathbf{r}_i e^{J_{n_i}(\lambda_i)t} \mathbf{l}_i x(0), \end{aligned} \tag{A.5}$$

and we are done.